Materials Research Proceedings 28 (2023) 1167-1174 https://doi.org/10.21741/9781644902479-127

Identification of the large strain flow curve of high strength steel via the torsion test and FEMU

VANCRAEYNEST Niels[1,a *], COOREMAN Steven[2,b] and COPPIETERS Sam[1,c]

[1]Elooi lab, Department of Materials Engineering, KU Leuven, KU Leuven-Gent Campus, Gebroeders De Smetstraat 1, 9000 Ghent, Belgium

[2] Applications & Solutions department, ArcelorMittal Global R&D Gent / OCAS NV, Belgium

[a]niels.vancraeynest@kuleuven.be, [b]steven.cooreman@arcelormittal.com, [c]sam.coppieters@kuleuven.be

Keywords: Large Strain Flow Curve, Torsion Test, Inverse Identification

Abstract. A torsion specimen is removed from the as-received thick high strength steel sheet (S700MC with a nominal thickness of 12 mm). The test material has a maximum uniform tensile strain of about 12 %. The torsion test is conducted up to fracture. The experimentally acquired torque-angle curve is then used to inversely identify the large strain flow curve up to an equivalent plastic strain of approximately 1. The identification strategy is based on the Finite Element Model Updating (FEMU) approach.

Introduction

Nowadays, numerical simulations are widely used in industry, hence generally considered to be a common engineering tool. However, the quality of simulations highly depends on the accuracy of the inputs. In metal forming simulations, it is well-known that the accuracy of the digital representation of the plastic material behaviour, i.e. the so-called material model, is of crucial importance for the predictive accuracy of the simulation. Commercially available finite element codes are still confined to phenomenological material models. In the case of metal plasticity, such models mostly rely on the concept of a yield surface, a hardening law and the associated flow rule. Experimental data is used to calibrate the governing material model parameters. Obviously, the type, quality and the amount of data determines the calibration accuracy. For example, the work hardening behaviour, also referred to as the flow curve, is conventionally calibrated using a standard tensile test in the Rolling Direction (RD). Since the majority of the metal forming processes generate plastic deformations beyond the maximum uniform tensile strain, the standard tensile test is of limited usefulness to determine the work hardening at large plastic strains, i.e. the large strain flow curve. In the case of sheet metal, several dedicated experiments enable to determine the large strain flow curve. Coppieters et al. [1] recently provided a comprehensive review on methods to determine the large strain flow curve of thin sheet metal. However, the majority of these methods cannot be applied to thick steel sheets. Zhang et al. [2] showed that it is possible to inversely extract the large strain flow curve from the diffuse neck in a tensile test. Alternatively, a torsion test can be used to probe large plastic strains without pronounced necking phenomena [3]. As opposed to a compression test, there is no influence of friction in the torsion test. To acquire the flow curve, the experimentally acquired torque-angle curve can be analytically converted to an equivalent stress-strain curve. The rotation angle directly yields the shear strain which is then converted to the equivalent plastic strain. However, for large plastic deformations, the validity of this analytical approach is violated since the relation between shear strain and equivalent strain does not remain linear [4,5]. The analytical post-processing is further complicated by the inhomogeneous stress and strain distribution within the torsion specimen. Indeed, the stress and strain radially increases in the cross section of the specimen. Thin-walled tubes circumvent

this problem, yet often buckle due to eccentricity of the inner and outer diameter or an unfavourable ratio between the wall thickness and radius [6]. Consequently, this work aims at extracting the post-necking work hardening behaviour of thick high-strength steel through a torsion test on a cylindrical bar. According to Petrov et al. [7], the analytical methods lack accuracy and it is recommended to inversely post-process the experimental data acquired during a torsion test. For example, Gavrus et al. [8] proposed a FEMU method to inversely identify the large strain flow curve. A similar approach is followed in this paper to identify a suitable phenomenological hardening law enabling to describe the pre- and post-necking hardening behaviour of a S700MC sheet with a nominal thickness of 12 mm. The paper is structured as follows. In the first section the experimental details of the torsion experiment are described. The second section embarks on the numerical counterpart of the torsion test. The third section introduces the FEMU method. In section four, the results are presented and discussed.

Experimental

The torsion test is conducted on a custom-made tension-torsion machine (see Fig 1). Consequently, one grip (twisting head) is able to rotate and the other grip (weighing head) is restricted to only translational movement along the rotation axis. The rotation is induced by a servo motor and the angle of rotation of the twisting head is measured with an internal encoder. At the weighing head, gripping the other side of the specimen, the twisting moment is measured using a piezoelectric load cell with a moment and tensile capacity of 100 Nm and 5 kN, respectively. To obtain a pure torsion test, the weighing grip is free to move along the rotation axis.

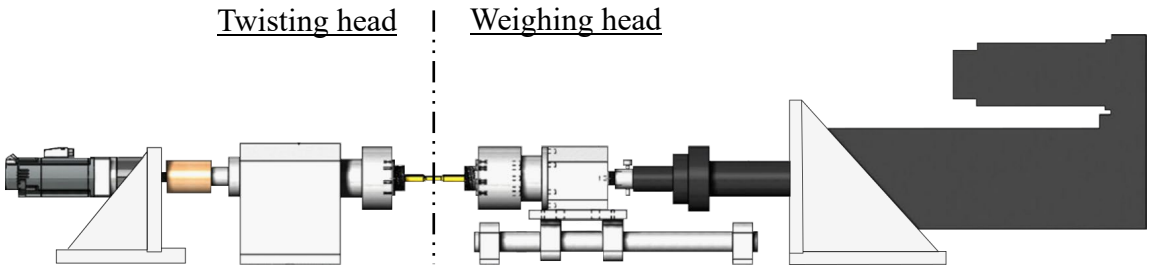

Fig. 1. Schematic overview of the tension-torsion machine. Left: Twisting head controlled by a servo motor; Right: Weighing head capable of measuring torque and tensile force with the possibility to connect a linear actuator to induce tension/compression.

The test material is a high strength low alloy (HSLA) steel S700MC with a nominal thickness of 12 mm. The ‘M’ and the ‘C’ indicate that the grade is made by a Thermomechanical Controlled Process (TMCP) and can be cold formed, respectively. Standard tensile tests were conducted and reported in [9], showing that the material exhibits a maximum uniform tensile strain of 0.12. The torsion samples are manufactured from the steel sheet in the RD. This is schematically visualized in the left panel of Fig. *2*. First, rectangular samples were removed by waterjet cutting. Through precision turning the final torsion samples were obtained as shown in the right panel of Fig. 2.

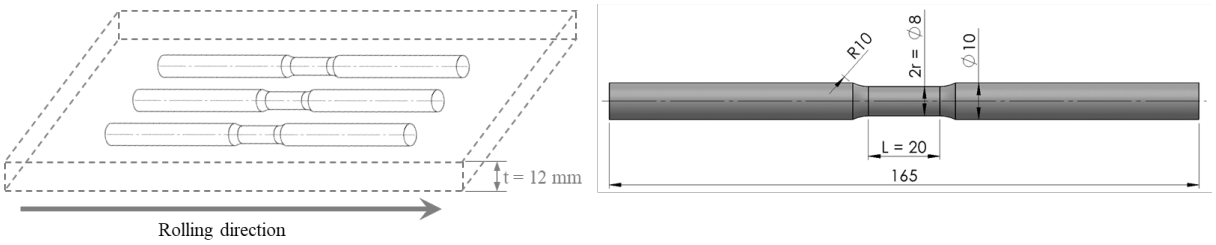

Fig. 2. The orientation of the torsion samples in the steel sheet (left) and geometry of the torsion sample after precision turning (right).

The torsion test is conducted under quasi-static conditions with a nominal strain rate in the order of $\dot{\varepsilon}_{eq} \approx 10^{-3}\frac{1}{s}$. For small rotational angles, the shear strain γ can be converted to the equivalent strain [4]:

$$\dot{\varepsilon}_{eq} = \frac{\dot{\gamma}}{\sqrt{3}} = \frac{r \cdot \dot{\theta}}{L \cdot \sqrt{3}} \tag{1}$$

With *r* the radius and *L* the length of the gauge section. $\dot{\theta}$ is the rotational speed of the twisting head. For the dimensions shown in the right panel of Fig. *2*, Eq. (1) yields a maximum rotational speed $\dot{\theta}$ of *30 °/min* to ensure quasi-static conditions. Three experiments were conducted using a constant speed of rotation *(20 °/min*) up to fracture of the sample. The results can be seen in Fig. *3*. The three repetitions are shown by the dashed grey lines. The solid black line is the average of the three experiments. All experiments easily reached *600* ° of rotation prior to fracture. Identical flat fracture surfaces perpendicular to the rotation axis were obtained in the three experiments.

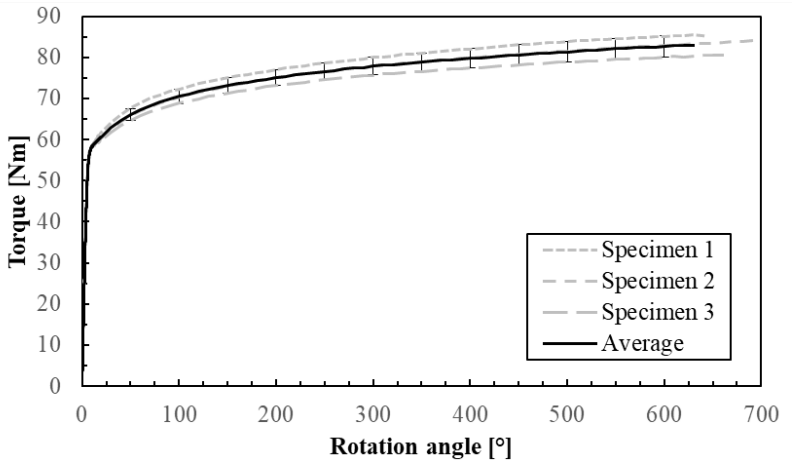

Fig. 3. Experimentally aquired Torque-rotation angle curves.

Numerical

The quasi-static torsion test is simulated using Abaqus/Standard. The torsion sample shown in the right panel of Fig. 2 is modelled in 3D using brick elements. The gripping areas are kinematically coupled with reference points onto which the boundary conditions are applied. The reference point referring to the twisting head is constrained in all degrees of freedom but the rotation angle. The reference point associated with the weighing head fixes all degrees of freedom but the translation along the rotation axis. The specimen is meshed with hexahedral elements (C3D8R) with an average size of 0.3 mm in the gauge section. The material is assumed to be elastically and plastically isotropic. Young's modulus and Poisson's ratio are assumed to be equal to 210GPa and 0.3, respectively. The plastic material behaviour is modelled using the von Mises yield criterion and a phenomenological hardening law.

It has been shown in [9] that the pre-necking hardening behaviour of S700MC can be accurately described by Swift's hardening law. Thus, Swift's hardening law can be fitted to pre-necking

hardening data acquired with a uniaxial tensile test (UTT). As opposed to Swift's hardening law, Voce's hardening law enables to predict saturation of the work hardening. Given that the large strain flow curve is a composite curve, several researchers proposed to combine existing hardening laws. An example of such approach is the p-model proposed by Coppieters and Kuwabara [10]. The p-model essentially combines Swift's and Voce's hardening and was recently successfully adopted to capture the large strain flow curve of 5182-O aluminium alloy [11].

Table 1. Selected phenomenological hardening laws.

Hardening law	Model description
Swift [12]	$\sigma_{eq} = K\left(\varepsilon_0 + \varepsilon_{eq}^{pl}\right)^n$
Voce [13]	$\sigma_{eq} = C\left[1 - me^{-B\varepsilon_{eq}^{pl}}\right]$
p-model [10]	$\sigma_{eq} = \begin{cases} K\left(\varepsilon_0 + \varepsilon_{eq}^{pl}\right)^n, & \varepsilon_{eq}^{pl} \le \varepsilon_{max} \\ K(\varepsilon_0 + \varepsilon_{max})^n + \frac{Kn(\varepsilon_0 + \varepsilon_{max})^{n-1}}{p}\left[1 - e^{-p\left(\varepsilon_{eq}^{pl} - \varepsilon_{max}\right)}\right], & \varepsilon_{eq}^{pl} > \varepsilon_{max} \end{cases}$

Table 1 summarises the hardening laws considered in this work. The model parameters will be inversely identified using FEMU. Swift's and Voce' hardening law both involve three unknowns. The p-model was constructed under the assumption that the large strain flow curve can be extracted from the diffuse neck in UTT. The pre-necking data is then readily available, hence the parameters $K, \varepsilon_0, \varepsilon_{max}$ and n are considered to be known and only the post-necking parameter p is subjected to inverse identification. To increase the flexibility of the p-model in the large strain range probed in the torsion test, however, p and ε_{max} are considered to be the unknown hardening parameters in this work. For the p-model, K, ε_0 and n are fixed and equal to the values found when fitting Swift to the pre-necking data of the UTT. Given that FEMU is driven by a gradient-based optimization, a good initial parameter guess is important to robustly identify the sought parameters. The pre-necking data of the UTT is used to determine the initial guess values, see Table 2.

Table 2. Initial guess values of the unknown hardening parameters.

Hardening law	Initial guess values
Swift	$K = 1250{,}62\ MPa\ ;\ \varepsilon_0 = 0{,}02409\ ;\ n = 0{,}1533$
Voce	$C = 1231{,}49\ ; m = 0{,}4012\ ;\ B = 3{,}52$
p-model	$p = 5\ ;\ \varepsilon_{max} = 0{,}15$

Finite Element Model Updating (FEMU)

With FEMU, the goal is to minimize the discrepancy between the experimental and numerical data and hereby inversely identifying the sought hardening parameters [7], [14]. To compare both datasets, here the torque-angle curves, a cost function $C(\boldsymbol{p})$ is used:

$$C(\boldsymbol{p}) = \frac{1}{2}\left[\boldsymbol{T}_{exp} - \boldsymbol{T}_{num}(\boldsymbol{p})\right]^T \cdot \left[\boldsymbol{T}_{exp} - \boldsymbol{T}_{num}(\boldsymbol{p})\right] \quad (2)$$

With $\boldsymbol{T}_{exp}$ and $\boldsymbol{T}_{num}(\boldsymbol{p})$ the column matrices of the torque for specific rotation angles obtained through the experiment and the FE model, respectively. The vector of the unknown parameters $\boldsymbol{p}$ is iteratively tuned to minimize $C(\boldsymbol{p})$.

To find a local minimum of $C(\boldsymbol{p})$, Cooreman [15] described two local optimization algorithms, namely Gauss-Newton and Levenberg-Marquardt. Both methods rely on the sensitivity matrix $\boldsymbol{S}$. This sensitivity matrix captures the influence of a parameter perturbation on the numerical response $\boldsymbol{T}_{num}$. The construction of the sensitivity matrix via finite differentiation requires an additional simulation per unknown parameter. The parameter update following Levenberg-Marquardt in each iteration reads as:

$$\Delta\boldsymbol{p} = [\boldsymbol{S}^T \cdot \boldsymbol{S} + \alpha \cdot \boldsymbol{I}]^{-1} \cdot \left[\boldsymbol{S}^T \cdot \left[\boldsymbol{T}_{exp} - \boldsymbol{T}_{num}\right]\right] \tag{3}$$

With α a scalar that is strictly positive. If α is zero, then the Gauss-Newton (GN) algorithm is retrieved. Levenberg-Marquardt (LM) is typically used to mitigate stability problems. The implemented optimization strategy follows the work of Denys [16] in which a combination of GN and LM is proposed. The FEMU starts with GN. While looping through the FEMU code the smallest value of the cost function $C(\boldsymbol{p}_{min})$ is stored in the memory. Upon the first increase of the cost function $C(\boldsymbol{p}_k)$ after a parameter update in iteration *k*, the optimization switches to the LM algorithm using an initial damping factor α equal to 10^{-7}. In iteration *(k+1)*, the parameters obtained in iteration (*k*-1) are used to predict the parameters update using LM. If $C(\boldsymbol{p}_{k+1})$ is lower than $C(\boldsymbol{p}_{min})$, the damping factor α will be divided by ten. Otherwise, α will be multiplied by ten to increase the damping behaviour. Convergence is assessed based on the relative change between the current and minimum cost function, $C(\boldsymbol{p})$ and $C_{min}(\boldsymbol{p})$, respectively. The FEMU code stops when the change is below 0.5 %.

Results

In a first step, the torsion test was simulated using Swift's hardening law calibrated based on the pre-necking data obtained from UTT. The parameters can be found in Table 2. The results are shown in Fig. 4 with the dotted line indicating the rotation angle where the maximum plastic strain in the simulation is equal to the maximum uniform tensile strain during the UTT. It can be inferred that the discrepancy with the experiment increases when the torsion test starts to probe strains beyond the maximum uniform tensile strain, i.e. beyond a rotation angle of approximately *75* °. This clearly indicates that the extrapolation of the hardening behaviour by Swift's hardening law is not valid, hence the need to identify the large strain flow curve based on experimental data beyond the maximum uniform tensile strain.

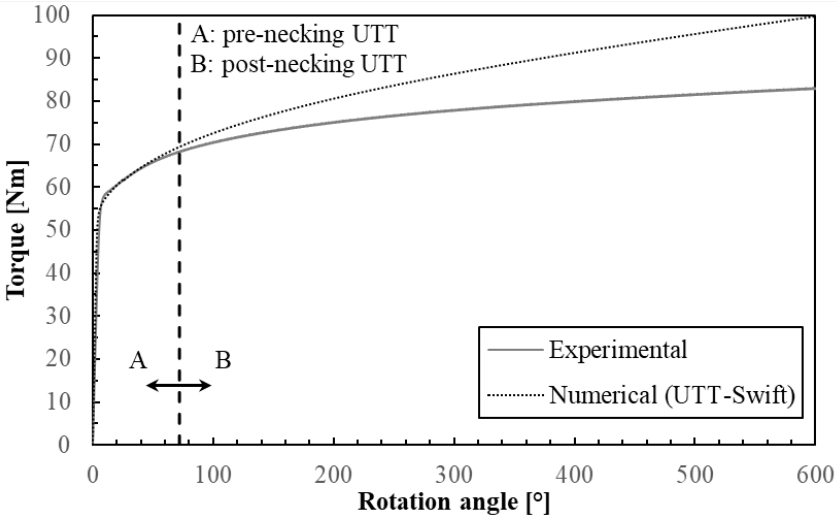

Fig. 4. Comparison between the experimental and the numerical torque-angle curve. With the material behaviour calibrated based on pre-necking data obtained from an UTT.

The FEMU code is fed with the torque-angle curve from 25° until 600°, ensuring that the torsion sample is sufficiently plastically deformed. The rotation angle of 25° is chosen arbitrarily and corresponds to a maximum ε_{eq}^{pl} of 0.04. The upper bound of 600° corresponds to a maximum ε_{eq}^{pl} of 1 without any visible damage. Each 2.5° of rotation, the torque value is probed to accurately capture the material response.

Table 3. The identified hardening parameters.

Hardening law	Hardening parameters	Accuracy Rank
Swift	$K = 1013{,}51\ MPa\ ;\ \varepsilon_0 = 0{,}003643\ ;\ n = 0{,}05792$	3
Voce	$C = 980{,}5754\ ; m = 0{,}2302\ ;\ B = 8{,}48$	1
p-model	$p = 13{,}65\ ;\ \varepsilon_{max} = 0{,}066$	2

The FEMU started with the initial parameters shown in Table 2. The inversely identified hardening parameters are shown in Table *3*. The accuracy rank shown in Table 3 is based on the value of the cost function upon convergence, also referred to as the cost function residual. The lower the cost function residual, the better the similarity between the experimentally acquired and numerically computed torque-angle curves. Consequently, the cost function residual gives an indication of the accuracy of the identified large strain flow curve. It can be inferred that Voce yields the lowest cost function residual, hence deemed to be the best choice for capturing the overall work hardening behaviour of S700MC during a torsion test. Fig. 5 shows the inversely identified hardening laws along with the extrapolated Swift law (UTT). It can be seen that the inversely identified hardening behaviour exhibits saturation at an equivalent stress of approximately 980MPa. Since Swift's hardening law cannot describe such saturation behaviour, and FEMU merely seeks for lowest cost function residual, a trade-off is found for the inversely identified Swift law. Indeed, the accuracy in the pre-necking region is lost to compensate for the inherent inaccuracy of Swift's hardening law in the post-necking regime. In this regard, the p-model is more flexible than Swift's hardening law. Nevertheless, the p-model cannot reproduce the Voce model in the complete strain range when only ε_{max} and p are considered to be the unknowns. Fig. 6 shows the predicted torque-rotation angle curve using the inversely identified hardening laws along with the experiment. It can be inferred that both the Swift law and the p-model predict an overshoot in a particular strain range, while Voce accurately predicts the experiment in the complete strain range.

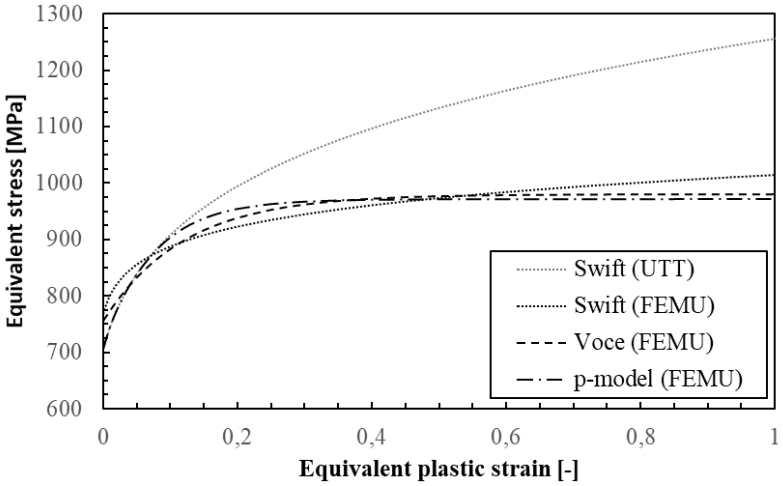

Fig. 5. The inversely identified flow curves compared with the extrapolated Swift law using the UTT.

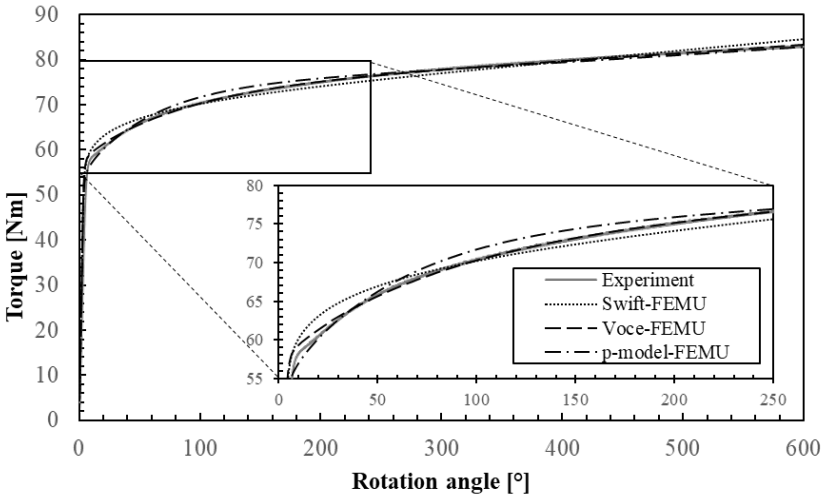

Fig. 6. Torque-rotation angle predicted by the FE model using the inversely identified hardening law. The solid grey line shows the experimental data.

Summary

The torsion test is used to inversely identify the large strain flow curve of a thick S700MC steel sheet. The FEMU approach uses the torque-twist curve to identify the parameters of three phenomenological work hardening laws. The methodology assumes the availability of a standard tensile test in the rolling direction to determine a reasonable initial guess of the sought parameters. It is shown that the hardening behaviour of S700MC, with a nominal thickness of 12mm, during a torsion test up to an equivalent plastic strain of 1 can be accurately described by Voce's hardening law. The following observations will be considered in future work:

- During the torsion test, limited spiral necking in the gauge length could be observed. It must be noted that the adopted FE model did not reproduce this phenomenon. It will be investigated if this is stemming from ignoring plastic anisotropy or an experimental error, e.g. an eccentricity problem.
- The influence of plastic anisotropy on the inverse identification of the large strain flow curve will be investigated.
- A multi-linear hardening law will be implemented to mitigate limitation imposed by the predefined character of phenomenological hardening laws.
- With a direct current potential drop (DCPD) measuring system, the objective is to determine the onset of damage. This would then enables to guarantee that only the undamaged part of the torque-twist curve is fed to the FEMU code.

Acknowledgements

This research was supported by the Research Fund for Coal and Steel under grant agreement No. 888153.

References

[1] S. Coppieters, H. Traphöner, F. Stiebert, T. Balan, T. Kuwabara, A.E. Tekkaya, Large strain flow curve identification for sheet metal, J. Mater. Process. Technol. 308 (2022) 117725. https://doi.org/10.1016/J.JMATPROTEC.2022.117725

[2] H. Zhang, S. Coppieters, C. Jiménez-Peña, D. Debruyne, Inverse identification of the post-necking work hardening behaviour of thick HSS through full-field strain measurements during diffuse necking, Mech. Mater. 129 (2019) 361-374. https://doi.org/10.1016/j.mechmat.2018.12.014

[3] M.V. Erpalov, E.A. Kungurov, Examination of Hardening Curves Definition Methods in Torsion Test, Solid State Phen. 284 (2018) 598. https://doi.org/10.4028/www.scientific.net/SSP.284.598
[4] N. Pardis, R. Ebrahimi, H.S. Kim, Equivalent strain at large shear deformation: Theoretical, numerical and finite element analysis, J. Appl. Res. Technol. 15 (2017) 442-448. https://doi.org/10.1016/j.jart.2017.05.002
[5] S.C. Shrivastava, J.J. Jonas, G. Canova, Equivalent strain in large deformation torsion testing : theoretical and practical considerations, J. Mech. Phys. Solids 30 (1982) 75-90. https://doi.org/10.1016/0022-5096(82)90014-X
[6] A.H. Stang, W. Ramberg, G. Back, Torsion Tests of Tubes, Jan. 1937, Accessed: Nov. 15, 2022. [Online]. Available: https://digital.library.unt.edu/ark:/67531/metadc66259/m1/14/
[7] P. Petrov, D. Shishkin, Y. Kalpin, I. Burlakov, S. Vydumkina, D. Kapitanenko, Determination of the flow curve based on the torsion of conical specimen, Procedia Manuf. 50 (2020) 520-528. https://doi.org/10.1016/J.PROMFG.2020.08.094
[8] A. Gavrus, E. Massoni, J.L. Chenot, An inverse analysis using a finite element model for identification of rheological parameters, J. Mater. Process. Technol. 60 (1996) 447-454. https://doi.org/10.1016/0924-0136(96)02369-2
[9] D. Debruyne et al., Towards Best Practice for Bolted Connections in High Strength Steels, 2019.
[10] S. Coppieters, T. Kuwabara, Identification of Post-Necking Hardening Phenomena in Ductile Sheet Metal, Exp. Mech. 54 (2014) 1355–1371. https://doi.org/10.1007/S11340-014-9900-4/FIGURES/16
[11] H. Shang, C. Zhang, S. Wang, Y. Lou, Large strain flow curve characterization considering strain rate and thermal effect for 5182-O aluminum alloy, Int. J. Mater. Forming 16 (2023) 1-20. https://doi.org/10.1007/S12289-022-01721-4/FIGURES/16
[12] H.W. Swift, Plastic instability under plane stress, J. Mech. Phys. Solids 1 (1952) 1-18. https://doi.org/10.1016/0022-5096(52)90002-1
[13] E. Voce, The relationship between stress and strain for homogeneous deformation, J. Inst. Metals 74 (1948) 537-562.
[14] M. di Donato, S. Bruschi, G. Hirt, M. Franzke, Flow curve determination by torsion tests using inverse modelling, 2016.
[15] S. Cooreman, Identification of the plastic material behaviour through full-field displacement measurements and inverse methods, PhD Thesis, VRIJE Universiteit Brussel, (2008).
[16] K. Denys, Investigation into the plastic material behaviour up to fracture of thick HSS using multi-DIC and FEMU, PhD Thesis, KU Leuven, (2017).